Probabilistic fragility analysis and resilience assessment of bridges subjected to earthquake mainshocks and aftershocks

I. Gidaris[1], J. E. Padgett[2]

[1] *Post-Doctoral Fellow, Department of Civil and Environmental Engineering, Rice University, 6100 Main St., Houston, TX 77005, ioannis.gidaris@rice.edu*

[2] *Associate Professor, Department of Civil and Environmental Engineering, Rice University, 6100 Main St., Houston, TX, 77005, jamie.padgett@rice.edu*

Abstract

Notable past seismic events, such as the 2010 Chile earthquake, the 2011 Tohoku earthquake in Japan and the seismic events in Christchurch, New Zealand in 2011, have shown that the mainshock seismic event can trigger sequences of aftershocks. In such cases the time between the primary shock and the aftershocks might be not enough for repairing the mainshock-induced damages to structures; hence their vulnerability can significantly increase and consequently their recovery is delayed. This issue can be even more critical for highway bridges that are one of the most vulnerable components of transportation networks when exposed to earthquakes, since the higher risk imposed due to the successive shocks can have devastating effects to entire communities relying on them for their smooth functioning. Therefore, it is important to develop methodologies that capture the impact of incorporating aftershocks in the seismic vulnerability and resilience of highway bridges. This paper discusses a computationally efficient methodology for probabilistic fragility analysis and resilience assessment of bridges that explicitly incorporates the effects of aftershock seismic events in the seismic hazard description. This methodology is based on nonlinear time-history analysis for simulating the structural response, whereas a procedure is developed for generating mainshock-aftershock sequences through stochastic ground motion modeling to support the mainshock-aftershock earthquake hazard characterization. In this setting, mainshock-induced damage state-dependent aftershock fragilities are developed, which are ultimately utilized in conjunction with appropriate recovery models for evaluation of bridge functionality and resilience. The various model parameters characterizing the seismic hazard, structural and recovery models are considered as uncertain, and the bridge performance metrics (i.e., fragility, functionality, resilience) are probabilistically calculated. To facilitate adoption of complex structural and probability models, an efficient computational framework based on kriging surrogate modeling is used for estimating the bridge performance metrics through stochastic (Monte Carlo) simulation. The surrogate model is established in an input parameter space, composed of uncertain seismic hazard and structural parameters, and deterministic structural/geometrical bridge parameters, and therefore is utilized to facilitate development of parameterized fragilities. As an illustrative example fragility and resilience assessment of a typical bridge class in California under the effects of mainshocks and aftershocks is performed.

Keywords: aftershock fragility, mainshock-aftershock sequences, probabilistic seismic resilience, kriging metamodeling

1. Introduction

Past experience (e.g. seismic events in Christchurch, New Zealand in 2011) as well as probabilistic analysis [1] have shown that the likelihood of a structure experiencing sequences of earthquake events such as mainshock and aftershocks is significant. In such cases it is likely that a bridge sustaining damages due to a mainshock event will not be repaired when subsequent aftershock events occur; hence its vulnerability can considerably increase and consequently its recovery is delayed, leading to reduction in the resilience of the bridge. Therefore, it is important to develop methodologies that capture the impact of incorporating aftershock events in the probabilistic fragility and resilience assessment of bridges. This topic has received limited attention so far, and the focus of relevant studies has been on specific bridge case studies [2-4] without considering uncertainties pertaining to hazard or bridge model parameters [2], using simplified (i.e., SDOF) models to evaluate seismic response [3, 4], or without explicitly subjecting the bridge model to mainshock-aftershock earthquake sequences [5]. This study seeks to advance these efforts and presents an efficient methodology for probabilistic fragility analysis and resilience assessment of bridges that explicitly incorporates the effects of aftershock events in the seismic hazard description and addresses various sources of uncertainty. Within this methodology the structural response is evaluated through nonlinear time history analysis, uncertainty is included in various structural and hazard model parameters; furthermore a seismic hazard characterization based on stochastic ground motion modeling is adopted supporting a method proposed for simulating mainshock-aftershock sequences. Sophisticated finite element models are employed to capture the highly inelastic behavior of the bridge subjected to mainshocks and aftershocks. Select engineering demand parameters (*EDP*s) are utilized to link the bridge's seismic response with damage states and ultimately evaluate damage state-dependent aftershock fragility, quantifying the conditional probability of meeting or exceeding a specified damage state given an intensity measure of the earthquake excitation and the initial mainshock-induced damage state. Then the estimated fragilities can be mapped to recovery models describing the percentage of the bridge's functionality as a function of the damage state attained and the time elapsed after the seismic event. Ultimately, knowledge of the functionality allows calculation of the resilience of a bridge. Because of the complexity of the adopted numerical and probability models, all required fragilities and resilience/functionality metrics are estimated through stochastic simulation, which can facilitate high-accuracy estimates, though frequently at a large computational burden. Therefore, in this study an efficient kriging surrogate modeling technique [6] is adopted to alleviate this burden. The surrogate model (known also as a metamodel) is developed for approximating the *EDPs* of interest with respect to various parameters that impact the seismic response (i.e. uncertain hazard and structural model parameters, and deterministic structural/geometrical bridge parameters), whereas the inherent stochastic characteristics of the earthquake ground motions are addressed through adoption of an appropriate statistical distribution for the *EDP*s under the influence of white noise. Such an input parameterization of the surrogate model facilitates an efficient development of parameterized fragilties. Once the metamodel is established, the fragility and resilience assessment are efficiently performed by stochastic simulation. In the illustrative example, the proposed methodology is implemented to a typical bridge class in California.

2. Mainshock and aftershock fragility analyses

In general, fragility is defined as the probability that a structure will meet or exceed a specified, i^{th}, damage state (*DS*) conditioned on a given intensity measure (*IM*) of the seismic hazard (e.g. peak ground acceleration). This conditional probability can be expressed as $P[DS \geq i \,|\, IM] = P[z \geq b_i \,|\, IM]$, where z denotes an *EDP*, corresponding to a bridge response quantity of interest (e.g. peak column drift, peak column displacement ductility, etc.), and b_i denotes a capacity threshold that determines initiation of the ith damage state. It is noted here that for the remainder of the paper superscripts *ms* and *as* characterize quantities/variables associated with mainshock and aftershock excitations, respectively.

2.1 Probabilistic quantification of mainshock seismic fragility

The evaluation of mainshock seismic bridge response z^{ms}, established here in terms of nonlinear time history analysis, which is ultimately required for quantification of fragility, entails adoption of appropriate excitation (i.e. seismic hazard) and bridge system models. These models are characterized by a set of uncertain model

parameters pertaining to the properties of the bridge system (e.g. material strengths) and/or characteristics of the excitation (e.g. duration of strong ground motion). In this context, let $\boldsymbol{\theta} \in \Theta$, denote a vector composed of all model parameters for the individual structural and excitation models, and Θ represents the space of possible model parameter values. Usually, these parameters are considered as uncertain variables characterized by a probability density function (PDF) $p(\boldsymbol{\theta})$. Furthermore, as discussed in the introduction, a stochastic ground motion model is adopted here as an excitation model, which involves as primary input a (Gaussian) white noise sequence, $\mathbf{w} \in W$ (more details for this model are provided in section 5). Similar to $\boldsymbol{\theta}$, the uncertainty in the white noise sequence $\mathbf{w}$ is described through a PDF denoted as $p_w(\mathbf{w})$. Within this probabilistic framework for evaluating structural response, seismic fragility for a bridge subjected to mainshock is quantified as:

$$P[DS^{ms} \geq i \mid IM^{ms}] = \int_{\Theta} \int_{W} P[z^{ms} \geq b_i \mid IM^{ms}, \boldsymbol{\theta}, \mathbf{w}] p_w(\mathbf{w}) p(\boldsymbol{\theta}) d\mathbf{w} d\boldsymbol{\theta} \tag{1}$$

In this definition it is common to introduce uncertainty in the damage state threshold by assuming that b_i follows a lognormal distribution [7]. This then leads to [6]:

$$P[z^{ms} \geq b_i \mid IM^{ms}, \boldsymbol{\theta}, \mathbf{w}] = \Phi\left[\ln(z^{ms} / b_i) / \sigma_b \mid IM^{ms}, \boldsymbol{\theta}, \mathbf{w}) \right] \tag{2}$$

where $\Phi(.)$ denotes the standard normal cumulative distribution function (CDF) and σ_b is the logarithmic standard deviation associated with b_i.

2.2 Probabilistic quantification of aftershock fragility for mainshock-damaged bridge

The formulation in the previous subsection described fragility quantification for intact bridges subjected to mainshock seismic events. However, bridges that are subjected to mainshock – aftershock earthquake sequences may sustain damages after the first shock. Hence, aftershock fragility for a damaged bridge should take into account the extent of the mainshock-induced damages. This state-dependent fragility is defined as the probability of meeting or exceeding the kth aftershock-induced damage state DS^{as} conditioned on the aftershock intensity measure IM^{as} and the initial mainshock-induced damage state $DS^{ms} = i$, and it is expressed as [8]:

$$\begin{aligned} &P[DS^{as} \geq k \mid IM^{as}, DS^{ms} = i] \\ &= \int_{\Theta} \int_{W} \int_{Z^{ms}} P[DS^{as} \geq k \mid IM^{as}, z^{ms}, \boldsymbol{\theta}, \mathbf{w}] p(z^{ms}, \boldsymbol{\theta} \mid DS^{ms} = i) p_w(\mathbf{w}) dz^{ms} d\mathbf{w} d\boldsymbol{\theta}; i, k \in [1, n_{ds}]; \ k \geq i \end{aligned} \tag{3}$$

where z^{ms} denotes the mainshock EDP and n_{ds} is the number of the considered DSs.

The first term of the integrand in Eq.(3), $P[DS^{as} \geq k \mid IM^{as}, z^{ms}, \boldsymbol{\theta}, \mathbf{w}]$, is the probability of reaching or exceeding damage state k given the mainshock response z^{ms}, which following similar considerations for threshold b_k as in section 2.1 can be expressed similar to Eq. (2) as $\Phi[\ln(z^{as} / b_k) / \sigma_b \mid IM^{as}, z^{ms}, \boldsymbol{\theta}, \mathbf{w})]$, where z^{as} denotes the response due to the aftershock event. Computation of the latter probability requires evaluation of z^{ms} and z^{as} through nonlinear time-history analysis of the bridge subjected to mainshock-aftershock sequences simulated through a procedure described in section 5. Finally, $p(z^{ms}, \boldsymbol{\theta} \mid DS^{ms} = i)$ denotes the joint PDF of z^{ms} and $\boldsymbol{\theta}$ conditioned on the case where bridge has reached the ith mainshock damage state.

Using the state-dependent fragility $P[DS^{as} \geq k \mid IM^{as}, DS^{ms} = i]$ in Eq. (3), the fragility of the bridge due to an aftershock event independent of the mainshock damage state can be evaluated through the use of the total probability theorem as [9]:

$$P[DS^{as} \geq k \mid IM^{as}] = \sum_{i=1}^{n_{ds}} P[DS^{as} \geq k \mid IM^{as}, DS^{ms} = i] P[DS^{ms} = i] \tag{4}$$

where $P[DS^{ms} = i] = P[DS^{ms} \geq i] - P[DS^{ms} \geq i+1]$ is the probability of being in the ith damage state, and $P[DS^{ms} \geq i]$ is evaluated by integrating the mainshock fragility in Eq. (1) over the probability distribution $p(IM^{ms})$ characterizing the mainshock seismic hazard:

$$P[DS^{ms} \geq i] = \int_{IM^{ms}} P[DS^{ms} \geq i \mid IM^{ms}] p(IM^{ms}) dIM^{ms} \tag{5}$$

Finally the probability that the bridge has reached the ith damage state either due to mainshock or aftershock is calculated as [5]:

$$P[DS = i \,|\, IM] = P[DS^{ms} = i \,|\, IM^{ms}] + \left(1 - P[DS^{ms} = i \,|\, IM^{ms}]\right) P[DS^{as} = i \,|\, IM^{as}] \tag{6}$$

where $P[DS^{as} = i \,|\, IM^{as}] = P[DS^{as} \geq i \,|\, IM^{as}] - P[DS^{as} \geq i+1 \,|\, IM^{as}]$.

3. Efficient fragility analysis through kriging surrogate modeling

Quantification of fragility as described in the previous section involves estimation of the bridge mainshock and aftershock seismic response through nonlinear dynamic analysis of sophisticated bridge finite element numerical models. Therefore, stochastic (Monte Carlo) simulation techniques are adopted for fragility calculation, which pose no constraints on the complexity of the numerical and probability models used. However, these simulation techniques can impose significant computational challenges rendering their implementation prohibitive, especially in the context of evaluating bridge response subjected to mainshock – aftershock sequences, since the structure can attain highly nonlinear levels of response due to the successive shocks. Moreover, the simulation time of the nonlinear time-history analysis is usually higher because of the significant duration of analysis with multiple seismic shocks; thus further increasing the required computational burden. Hence, for efficiently estimating fragility the kriging surrogate modeling framework presented in [6] is adopted for approximating the bridge mainshock z^{ms} and aftershock z^{as} response corresponding here to peak component response quantities such as column displacement ductility, with respect to a vector of input model parameters $\mathbf{x}$. Surrogate models are developed for approximating both z^{ms} and z^{as}, abbreviated *MS* and *AS*, respectively. For *MS* vector $\mathbf{x} = [IM^{ms} \, \boldsymbol{\theta} \, \mathbf{p}]$ is composed by mainshock intensity measure IM^{ms}, uncertain model parameters $\boldsymbol{\theta}$ and deterministic bridge geometric and/or structural parameters $\mathbf{p}$ such as column reinforcement ratio and/or span length, whereas for *AS* $\mathbf{x}$ is further augmented with mainshock response z^{ms} such that the history of the response prior to the aftershock is considered, and the aftershock intensity measure IM^{as} replaces IM^{ms}, i.e., $\mathbf{x} = [IM^{as} \, \boldsymbol{\theta} \, \mathbf{p} \, z^{ms}]$.

3.1 Statistical approximation of white noise and kriging formulation

The influence of the white noise sequence $\mathbf{w}$ involved in the ground motion model is addressed through a statistical approximation such that development of a surrogate model in a high-dimensional space (that would involve augmentation of $\mathbf{x}$ with $\mathbf{w}$) is avoided. Following recommendations in [6] this statistical approximation is established by assuming that, under the influence of white noise, response z^q; $q = ms$, as, follows a lognormal distribution with logarithmic mean $\ln(\overline{z}^q)$ and logarithmic standard deviation σ_{z^q}. This approximation is a common assumption in earthquake engineering [10].

The kriging surrogate model is formulated to provide predictions for the quantities needed to support evaluation of fragility, corresponding to the statistics of the mainshock and aftershock responses. These quantities define the output vector $\mathbf{y} = [\ln(\overline{z}^q) \, \sigma_{z^q}]$; $q = ms$, as. Details for the surrogate model development may be found in [6]. The process starts by generating n_m samples for $\{\mathbf{x}^l, l=1,\ldots,n_m\}$, also known as support points, following initially a Latin hybercube grid over the expected range of values possible for each component of $\mathbf{x}$. Stochastic ground motions are then generated according to the excitation model described in section 5 and the structural response is numerically evaluated. The influence of the white noise is addressed by considering n_w different samples for each $\mathbf{x}^l$ and using the statistics under these samples to ultimately quantify the response sample $\mathbf{y}^l$. Using this dataset for the input-output pair $\mathbf{x}$-$\mathbf{y}$ the kriging model is then obtained. When developing metamodel *AS* the logarithmic mean $\ln(\overline{z}^{ms})$ is used for the mainshock response z^{ms} component of $\mathbf{x}$.

Using this dataset the kriging surrogate model is developed providing the approximation of $\mathbf{y}$ which is associated with a prediction error that is a zero mean normal variable [6]. The approximation for $\ln(\overline{z}^q)$ can be expressed as $\ln(\overline{z}^q) = \ln(\hat{\overline{z}}^q) + \varepsilon^q$, where $\ln(\hat{\overline{z}}^q)$ is the kriging prediction of $\ln(\overline{z}^q)$ and ε^q is the associated prediction error with standard deviation σ_{ε^q}, whereas the prediction error for σ_{z^q} can be neglected following recommendations in [6]. Ultimately, under the lognormal assumption for white noise influence and incorporating the kriging prediction error, the probabilistic integrals in Eq. (1) and (3) for evaluating mainshock and aftershock fragility, respectively, simplify to (influence of $\mathbf{w}$ removed) [6]:

$$P[DS^{ms} \geq i \,|\, IM] = \int_{\Theta} \Phi \left[\frac{\ln(\overline{z}^{ms} / b_i)}{\sqrt{\sigma_b^2 + \sigma_{z^{ms}}^2 + \sigma_{\varepsilon^{ms}}^2}} \,\bigg|\, IM^{ms}, \boldsymbol{\theta} \right] p(\boldsymbol{\theta}) d\boldsymbol{\theta} \tag{7}$$

$$P[DS^{as} \geq k \mid IM^{as}, DS^{ms} = i] = \int_{\Theta} \int_{Z^{ms}} \Phi \left[\frac{\ln(\overline{z}^{as} / b_k)}{\sqrt{\sigma_b^2 + \sigma_{z^{as}}^2 + \sigma_{\varepsilon^{as}}^2}} \mid IM^{as}, \overline{z}^{ms}, \boldsymbol{\theta} \right] p(\overline{z}^{ms}, \boldsymbol{\theta} \mid DS^{ms} = i) d\overline{z}^{ms} d\boldsymbol{\theta} \quad (8)$$

3.2 Computational details for fragility calculation

The probabilistic integrals in Eq. (7) and (8) for evaluating of mainshock and aftershock fragility, respectively, are estimated through stochastic simulation utilizing the kriging surrogate model for a computationally efficient evaluation. In particular, using a finite number of samples, N, of $\boldsymbol{\theta}$ drawn from $p(\boldsymbol{\theta})$ with $\boldsymbol{\theta}^j$ denoting the jth sample, an approximation for the integral in Eq. (7) is given by:

$$\hat{P}[DS^{ms} \geq i \mid IM] = \frac{1}{N} \sum_{j=1}^{N} \Phi \left[\frac{\ln(\overline{z}^{ms} / b_i)}{\sqrt{\sigma_b^2 + \sigma_{z^{ms}}^2 + \sigma_{\varepsilon^{ms}}^2}} \mid IM^{ms}, \boldsymbol{\theta}^j \right] \quad (9)$$

Similarly, the integral in Eq. (8) is approximated as:

$$\hat{P}[DS^{as} \geq k \mid IM^{as}, DS^{ms} = i] = \frac{1}{N} \sum_{j=1}^{N} \Phi \left[\frac{\ln(\overline{z}^{as} / b_k)}{\sqrt{\sigma_b^2 + \sigma_{z^{as}}^2 + \sigma_{\varepsilon^{as}}^2}} \mid IM^{as}, \overline{z}^{ms,j}, \boldsymbol{\theta}^j \right] \quad (10)$$

where $\boldsymbol{\theta}^j$ and $\overline{z}^{ms,j}$ denote the jth samples drawn from $p(\overline{z}^{ms}, \boldsymbol{\theta} \mid DS^{ms} = i)$. Sampling from the latter distribution, which in general does not correspond to a known PDF, is performed by the following procedure. First, the population of samples from $[\overline{z}^{ms} \ \boldsymbol{\theta}]$ that led the bridge to $DS^{ms} = i$ is identified. This is accomplished by identifying the samples of $\overline{z}^{ms}$ and the associated ones for $\boldsymbol{\theta}$ that lie on the interval between b_i and b_{i+1}, i.e., $\overline{z}^{ms} \in [b_i \quad b_{i+1})$. Then based on these samples an approximation for $p(\overline{z}^{ms}, \boldsymbol{\theta} \mid DS^{ms} = i)$ is obtained through multivariate kernel density estimation (KDE) [11]. Finally, samples of $[\overline{z}^{ms} \ \boldsymbol{\theta}]$ from the joint density $p(\overline{z}^{ms}, \boldsymbol{\theta} \mid DS^{ms} = i)$ estimated through KDE are drawn through a stochastic sampling approach as in [12, 13].

4. Probabilistic resilience assessment

Quantification of fragility of a bridge under mainshock and mainshock-aftershock seismic hazard as discussed in the previous section can facilitate evaluation of its functionality and ultimately its resilience after the occurrence of one (or more) shocks. Here the time-variant functionality $Q(t)$ of a bridge can be expressed as [3]:

$$Q(t) = \sum_{i=1}^{n_{ds}} Q(t \mid DS = i) P[DS = i \mid IM] \quad (11)$$

where $Q(t|DS=i)$ denotes the functionality of the bridge conditional on the ith damage state. This quantity can be mathematically expressed as:

$$Q(t \mid DS = i) = Q_r + H(t - t_0 - \delta_i) f\left(t \mid DS = i\right)\left(Q_t - Q_r\right) \quad (12)$$

where t_0 is the time of occurrence of the seismic event, and Q_r is the residual functionality after the event occurrence. $H(.)$ represents the Heaviside step function, Q_t is the functionality reached at the end of the recovery process, δ_i is the idle time between the occurrence of the seismic event and the beginning of the recovery process and $f(.)$ is a restoration function describing the profile of the recovery process. A characteristic illustration of the variation of functionality with respect to time is shown in Fig. 1.

The second term in Eq. (11) denotes the probability of the bridge being in damage state i. For the case that only the mainshock hazard is considered the latter probability is equal to $P[DS^{ms} = i \mid IM^{ms}] = P[DS^{ms} \geq i \mid IM^{ms}] - P[DS^{ms} \geq i+1 \mid IM^{ms}]$. When the aftershock hazard is additionally considered this probability corresponds to the probability that that the specified damage state is reached either due to mainshock or aftershock, and it is calculated according to Eq. (6). It is noted that the assumption that no repair actions of the bridge are performed between the occurrence of mainshock and aftershock is made here for the calculation of functionality due to mainshock and aftershock hazard.
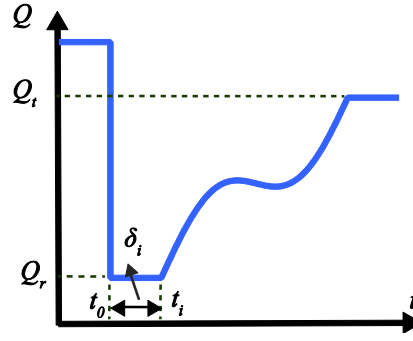
Fig. 1 - Characteristic representation of functionality evolution over time.

After bridge functionality is calculated through Eq. (11), the resilience of the bridge under a specified time horizon t_h can be quantified through the following definition [3]:

$$R = 1/t_h \int_{t_0}^{t_0+t_h} Q(t)dt \qquad (13)$$

It is noted that alternative definitions exist in the relevant literature [14].

Finally, for a fully probabilistic resilience assessment the functionality and resilience of a bridge must be calculated by taking into account uncertainties pertaining to the seismic hazard as well as the various parameters that are characterizing the damage state-dependent functionality in Eq. (12) [e.g., δ_i, Q_r, parameters defining $f(.)$, etc.]. If $\varphi \in \Phi$ denotes the vector of these parameters and $p(\varphi)$ corresponds to the PDF adopted to describe their uncertainty, the expected value of the bridge functionality and resilience is expressed through Eq.(14) and (15), respectively:

$$E[Q(t)] = \int_{IM} \int_{\Phi} Q(t) p(\mathbf{IM}) p(\varphi) d\mathbf{IM} d\varphi \qquad (14)$$

$$E[R] = \int_{IM} \int_{\Phi} R p(\mathbf{IM}) p(\varphi) d\mathbf{IM} d\varphi \qquad (15)$$

where $\mathbf{IM} = [IM^{ms} \ IM^{as}]$ and $p(\mathbf{IM})$ is the joint PDF characterizing the mainshock-aftershock hazard. It is noted that for the case when only mainshocks are considered $\mathbf{IM} \equiv IM^{ms}$. Ultimately, the probabilistic integrals in Eq. (14) and (15) are estimated through stochastic simulation in a similar way as described in section 3.2.

5. Excitation model and simulation of mainshock-aftershock sequences

For describing the seismic hazard a stochastic ground motion model [15] is adopted here, as discussed in previous sections. The approach involves as inputs two seismological parameters, the moment magnitude M and the rupture distance r, as well as predictive relationships that relate ground motion characteristics to these parameters. In particular, the excitation is represented through a point-source stochastic ground motion model [16] that entails modulation of the white noise sequence $\mathbf{w}$ through functions, dependent upon M and r, that address the frequency and time-domain characteristics of the excitation. Further details for the excitation model can be found in [17].

The effect of aftershock seismic events on the structural response and ultimately to fragility and resilience is taken into account in this study by subjecting the structural model to mainshock – aftershock sequences and performing nonlinear time-history analysis. A method for generating mainshock – aftershock sequences is developed in this paper that utilizes the point-source stochastic ground motion model briefly described above. In this method only one aftershock is considered for the sake of simplicity, as previous studies have shown that such as an assumption provides an acceptable balance between computational effort and accuracy [18]. The proposed process for mainshock –aftershock simulation is illustrated through a schematic flowchart in Fig. 2 and is composed by the following steps. First, a scenario for the mainshock seismic event is determined through the mainshock moment magnitude M^{ms} and rupture distance r^{ms} [part (a) in Fig. 2]. Then an aftershock scenario, which should be related with the mainshock event, is determined (e.g., using a Gutenberg-Ricther relationship

[23]) [part (b) in Fig. 2], by considering that the largest possible aftershock in terms of magnitude $M^{as}_{\max}$ is equal to M^{ms} [19], whereas the location of the mainshock and aftershock is assumed to be the same, i.e., $r^{ms} = r^{as}$ [20]. It is noted that the latter assumption is made for simplicity and more detailed considerations [21] can be incorporated in the method in a straightforward manner. After the scenarios for the mainshock and aftershock are determined acceleration time-history realizations are generated based on them through the adopted stochastic ground motion model [part (c) in Fig. 2]. Finally, a mainshock – aftershock sequence is obtained by assembling the aftershock acceleration time-history following the mainshock one with a time lag between them [part (d) in Fig. 2]. It is mentioned here that during this process appropriate intensity measures for the mainshock IM^{ms} and aftershock IM^{as} acceleration time-history realizations are computed and used in the input parameter vector **x** of the metamodels to characterize the intensity of the hazard. Ultimately, a probabilistic characterization (discussed in the example section) of M^{ms}, M^{as}, r^{ms} and r^{as} (based on the regional seismicity) supports then a comprehensive description of the seismic hazard.
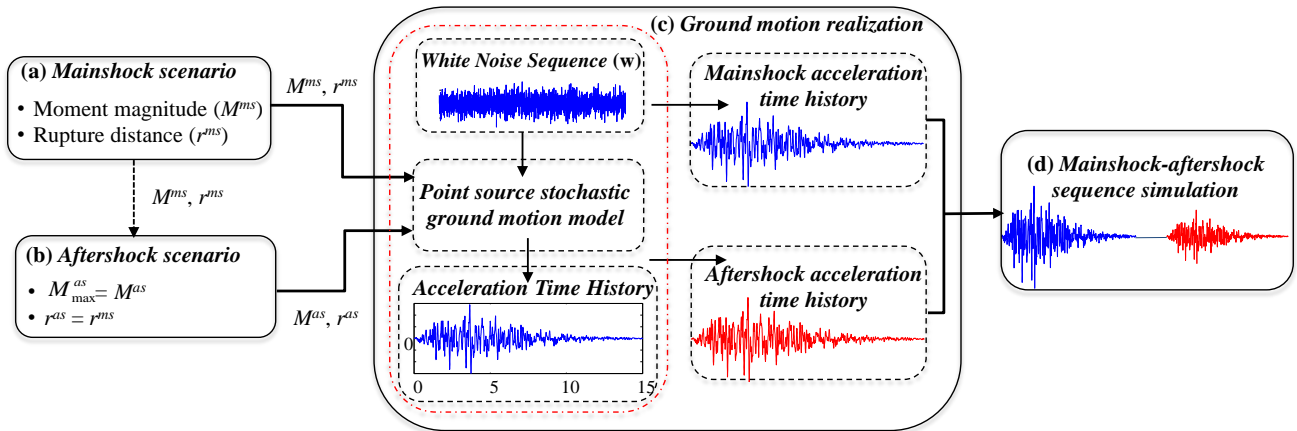
Fig. 2 **-** Schematic flowchart of the mainshock-aftershock sequence simulation process

6. Illustrative example

6.1 Structural and excitation models

For the illustrative example, a two span continuous reinforced concrete box girder bridge with integral abutments, which is a common bridge class in California [22], is considered and shown in Fig. 3. The bridge consists of two spans with equal length L, a circular column pier with height H_c, diameter D_c and longitudinal reinforcement ration ρ_s supported on a pile foundation, a deck with width W_d and two abutments supported by piles. Values of these geometrical parameters of the bridge are shown in Fig. 3 and correspond to common values for this bridge class [22].
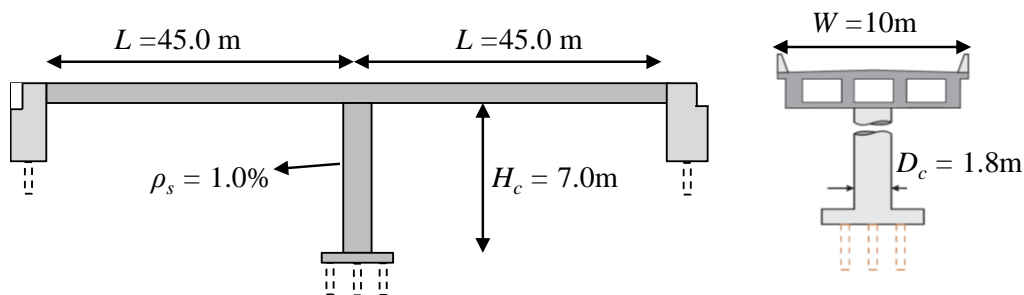
Fig. 3 – Layout of the bridge considered in the example.

A 3D finite element bridge model is developed in OpenSees following modeling recommendations in [22]. In particular, the superstructure is modeled with elastic beam-column elements with mass lumped along the centerline, whereas the column is modeled through discretized fiber cross sections applied to a beam-column element. The constitutive material laws for concrete and steel were *Concrete02* and *Hysteretic*, respectively.

Concrete and steel material strengths are denoted as f_c and f_s, respectively. The pile foundation of the pier is modeled with linear translational and rotational springs with stiffness values K_t and K_r respectively. The abutment active and passive response is modeled through nonlinear springs and the *Hysteretic* and *HyperbolicGapMaterial* laws, respectively. The primary model parameters for characterizing these laws are the effective abutment pile stiffness K_p and the initial backfill soil stiffness K_s. Rayleigh damping with damping ratio ζ associated with the first two modes is considered, and a multiplicative factor m_{add} is applied to the mass stemming from the dead weight such that additional sources of mass (e.g. live loads) are considered. A more detailed description of the assumptions and the analytical models can be found in [22]. All the above bridge parameters are considered uncertain with PDFs reported in Table 1.

Table 1 – Probability distributions for the uncertain bridge parameters

Parameter	PDF	PDF parameters[+]		Parameter	PDF	PDF parameters[+]	
		α	β			α	β
f_c (MPa)	Normal	34.5	4.34	K_t (kN/m)	Trun. Normal[*]	264165	105071
f_s (MPa)	Lognormal	465	0.08	K_r (kN/rad)	Trun. Normal[*]	7344000	1129800
ζ (%)	Lognormal	5.0	0.3	K_p (kN/m)	Lognormal	7000	0.2
m_{add}	Uniform	1.1	1.4	K_s (kN/m)	Lognormal	20300	0.2

[+] α and β represent parameters of the respective distribution, denoting mean and standard deviation for Normal, median and coefficient of variation for lognormal and lower and upper bound for uniform.

[*] Left truncated normal distribution with lower bound equal to one and five times the standard deviation for K_t and K_r, respectively [22].

For the excitation model, the uncertainty in the moment magnitude is modeled by the Gutenberg-Richter (G-R) relationship [23] truncated on the intervals [5.5 8.0] and [5.5 M^{ms}] for mainshocks and aftershocks, respectively. The regional seismicity parameters characterizing the G-R law are taken to be 0.90ln(10) and 0.91ln(10) for mainshocks and aftershocks, respectively [18]. Regarding the uncertainty in the event location, the rupture distance $r^{ms} = r^{as}$, is assumed to follow a lognormal distribution with median value 10 km and coefficient of variation 40%. Through such a probabilistic modeling of M^{ms}, M^{as} and $r^{ms} = r^{as}$, a probabilistic characterization of IM^{ms} and IM^{as} is also obtained. In this example, the peak ground acceleration (*PGA*) is used as intensity measure.

6.2 Surrogate model development details

As discussed in section 3 two separate surrogate models, *MS* and *AS*, are developed for approximating mainshock and aftershock response. The uncertain model parameters $\boldsymbol{\theta}$ that are used for establishing the metamodels are $\boldsymbol{\theta} = [f_c\, f_s\, \zeta\, m_{add}\, K_t\, K_r\, K_p\, K_s]$. It is noted that the seismological parameters M^{ms}, M^{as}, r^{ms} and r^{as}, characterizing the excitation model are not included in $\boldsymbol{\theta}$ since the intensity level of the ground motions is described through IM^{ms} and IM^{as}. However, for a different risk and/or resilience assessment application that the explicit dependence on *IM* is not required, vector $\boldsymbol{\theta}$ can be easily augmented with these seismological parameters [6]. Vector $\mathbf{p}$ of bridge structural and geometric deterministic parameters corresponds to $\mathbf{p} = [L\, H_c\, D_c\, \rho_s\, W_d]$. Therefore, the augmented input vector $\mathbf{x}$ is composed of $\boldsymbol{\theta}$, $\mathbf{p}$, IM^{ms} or IM^{as} as well as $\ln(\overline{z}^{ms})$ (for *AS* metamodel only), and it corresponds to $\mathbf{x} = [IM^{ms}\, f_c\, f_s\, \zeta\, m_{add}\, K_t\, K_r\, K_p\, K_s\, L\, H_c\, D_c\, \rho_s\, W_d]$ ($n_x = 14$ parameters) and $\mathbf{x} = [IM^{as}\, f_c\, f_s\, \zeta\, m_{add}\, K_t\, K_r\, K_p\, K_s\, L\, H_c\, D_c\, \rho_s\, W_d\, \ln(\overline{z}^{ms})]$ ($n_x = 15$ parameters), for *MS* and *AS*, respectively. A total of $n_m = 2000$ support points is used and the influence of the white noise is addressed by considering $n_w = 50$ samples. Space filling Latin hypercube sampling is used for the support points in the range that are expected to take values based on the assumed probability models for $\boldsymbol{\theta}$, whereas for the components of $\mathbf{p}$ appropriate ranges for this bridge class based on previous studies [22] are adopted. The response quantities z^{ms} and z^{as} predicted from the surrogate model correspond to the peak displacement ductilities of the column across the two orthogonal directions. The accuracy of the developed metamodels is evaluated by calculating different error statistics using the leave-one-out cross-validation approach. The accuracy established is adequately high with coefficient of determination over 90% and mean error less than 15% for most approximated response quantities, i.e. $[\ln(\overline{z}^q)\, \sigma_{z^q}]$; $q = ms, as$.

6.3 Fragility and functionality/resilience calculation details

The damage states that are used in this example are qualitatively described as slight, moderate, extensive and complete. The thresholds b_i determining the onset of these damage states for similar concrete bridge columns are adopted from the relevant literature [24] and are equal to 1.0, 1.20, 1.76, and 4.76, whereas σ_b is taken equal to 0.35. Fragility is evaluated by using the maximum value of peak displacement ductility between the two orthogonal directions for z^{ms} and z^{as}. For estimation of mainshock and aftershock fragility through stochastic simulation [Eq. (9) and (10)] a total of $N = 5000$ samples is used. Regarding, the model parameters for functionality evaluation through Eq. (12), target functionality Q_t is considered equal to 1, whereas the residual functionality Q_r and the idle time δ_i are considered as uncertain parameters composing vector $\boldsymbol{\varphi}$ with probability models adopted following recommendations in [25]. For the restoration function $f(.)$ in Eq. (12) the normal CDF shape as proposed in [26] is adopted. The total time horizon t_h for evaluation of resilience in Eq. (13) is taken here equal to 600 days. Finally, the same number of samples N is used for estimation of $E[Q(t)]$ and $E[R]$ through stochastic simulation.

6.4 Results and discussion

Using the kriging surrogate models established for approximating the bridge nonlinear response for the realizations of parameters composing **p** reported in Fig. 3 and the adopted probability models for the various model parameters, mainshock and state-dependent aftershock fragilities as well as expected functionality and resilience of the bridge under study are estimated through stochastic simulation. In particular, Fig. 4 presents the aftershock fragilities $\hat{P}[DS^{as} \geq k \mid IM^{as}, DS^{ms} = i]$ for the four damage states considered estimated through stochastic simulation [Eq. (10)]. Parts (a), (b), (c) and (d) of the figure correspond to aftershock damage states DS^{as} = slight, moderate, extensive and complete, respectively. The different curves for each sub-plot indicate different levels of damage induced by the mainshock, whereas the curve reported as "intact" in the legend corresponds to the mainshock fragility $\hat{P}[DS^{ms} \geq i \mid IM]$ estimated through Eq. (9). Comparing the mainshock and aftershock fragilities it is evident that inclusion of aftershock events in the seismic hazard description leads to increased vulnerability of the bridge as it was expected. Moreover, the effect of different levels of mainshock-induced damage to the bridge can be observed through comparison of the different aftershock fragilities. It can be seen that as the bridge sustains more severe levels of damage due to the mainshocks the corresponding aftershock fragility increases. This result reveals the importance of incorporating aftershocks in the seismic hazard, since seismic risk is increased and consequently functionality and resilience of the bridge is reduced as demonstrated next.
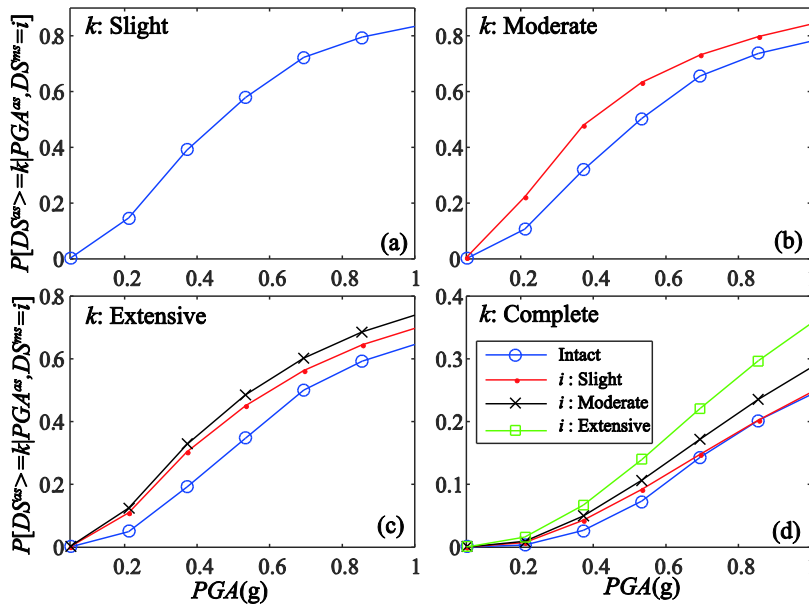
Fig. 4 – State-dependent aftershock fragilities of the bridge under study

Moving now to the investigation of the impact of including aftershocks on functionality and resilience of the bridge, Fig. 5 presents the evolution of the expected functionality $E[Q(t)]$ with respect to time after seismic shock occurrence for the two hazard descriptions, i.e., including or disregarding aftershock events. The expected functionality is calculated by estimating the probabilistic integral in Eq. (14) via stochastic simulation. It can be observed that aftershock events can have a significant negative impact on the expected functionality of the bridge. As time evolves the difference of the expected functionality between the two cases is reduced, and ultimately the two curves converge to values of 1.0 that represent full restoration of the bridge. This result is attributed to the shape of the restoration curves $f(.)$ used in Eq. (12), since they rapidly increase as time evolves.
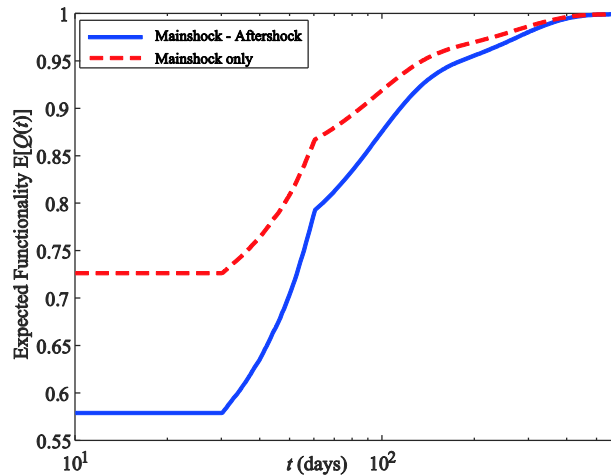
Fig. 5 – Expected functionality of the bridge for seismic hazard including or not aftershock events.

Calculation of the evolution of functionality can ultimately support evaluation of the expected resilience $E[R]$ of the bridge through stochastic simulation-based estimation of Eq. (15). Table 2 reports values of $E[R]$ for both hazard cases and for different time instants of the recovery phase of the bridge. The different time instants considered correspond to the total time horizon, i.e., $t_h = 600$ days, as well as to the intermediate instants $t_h = 45$, 60, 90 and 300 days. The percentage difference between the values of $E[R]$ for the two hazard cases is reported in parentheses. The results indicate the significant impact that aftershock events impose on the recovery of the bridge, since the expected resilience can be up to ≈20% smaller compared to the case that only mainshock events are considered.

Table 2 – Expected resilience $E[R]$ of the bridge calculated at different time instants of the recovery phase.

t_h (days)	$E[R]$		t_h (days)	$E[R]$	
	Mainshock	Mainshock- aftershock		Mainshock	Mainshock- aftershock
45	0.721	0.582 (19.4%)	300	0.913	0.868 (4.94%)
60	0.748	0.620 (17.2%)	600	0.955	0.932 (2.44%)
90	0.794	0.687 (13.5%)			

Finally, Fig. 6 presents histograms of the functionality samples of the bridge for different time instants (t = 45, 60, 90, 300 days) for both hazard cases. The mean values and the coefficient of variation (cov) of the samples are also reported. Beyond the expected trend (shown also in Fig. 5) of the reduced functionality when aftershocks are considered, it is interesting to observe that the cov for the mainshock-aftershock hazard is always higher than the mainshock case, and that for both cases the cov decreases as time evolves. The former trend is attributed to the fact that the incorporation of aftershocks in the hazard description introduces additional uncertainty. Whereas the latter trend is attributed to the fact that as mentioned above the particular shape of the restoration functions used leading to high values of functionality with small dispersion for higher time instants,

and that the parameters related to the functionality model considered as uncertain (i.e. Q_r, δ_i) influence the earlier part of the recovery process.
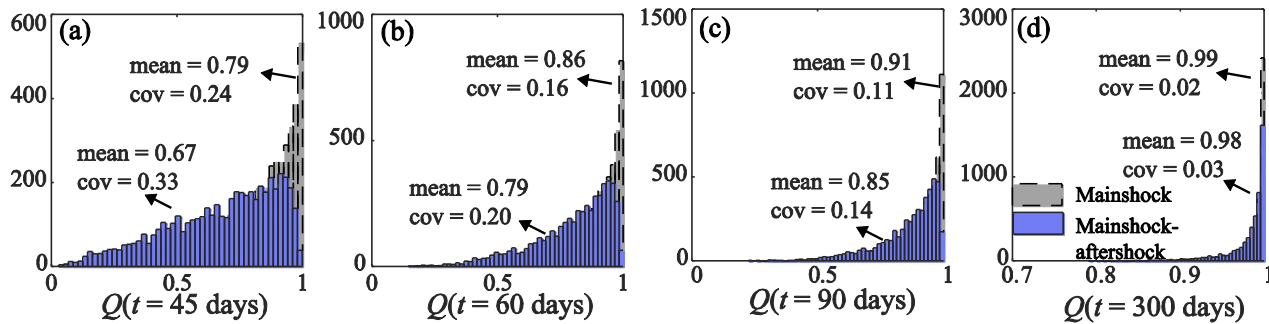
Fig. 6 – Histograms of functionality samples for different time instants of recovery phase. The mean values and the cov of the samples are also reported.

7. Conclusions

A computationally efficient methodology based on kriging surrogate modeling for probabilistic fragility and resilience analysis of bridges subjected to mainshock and aftershock seismic events is presented in this paper. The effect of aftershocks is explicitly considered by developing a procedure for simulating mainshock-aftershock sequences using stochastic ground motion modeling, and ultimately incorporating it in the mainshock-aftershock seismic hazard description. Approximation of the nonlinear mainshock and aftershock bridge response is obtained using the surrogate models established with respect to uncertain hazard and structural model parameters, deterministic bridge and geometrical parameters, and the mainshock response (when estimating aftershock response). These metamodels facilitate the development of parameterized mainshock and state-dependent aftershock fragilities and ultimately support investigation of the impact of aftershocks on the probabilistic resilience assessment of bridges. The examined example that considers a typical bridge class in California, illustrated that aftershocks can have a significant negative influence on the vulnerability and functionality of the bridge.

8. References

[1] Kumar R, Gardoni P (2011): Modeling structural degradation of RC bridge columns subjected to earthquakes and their fragility estimates. *Journal of Structural Engineering*.**138** (1):42-51.

[2] Jeon JS, DesRoches R, Lee DH (2016): Post-repair effect of column jackets on aftershock fragilities of damaged RC bridges subjected to successive earthquakes. *Earthquake Engineering & Structural Dynamics*.

[3] Dong Y, Frangopol DM (2015): Risk and resilience assessment of bridges under mainshock and aftershocks incorporating uncertainties. *Engineering Structures*.**83**:198-208.

[4] Ghosh J, Padgett JE, Sánchez-Silva M (2015): Seismic Damage Accumulation in Highway Bridges in Earthquake-Prone Regions. *Earthquake Spectra*.**31** (1):115-35.

[5] Kumar R, Gardoni P (2014): Effect of seismic degradation on the fragility of reinforced concrete bridges. *Engineering Structures*.**79**:267-75.

[6] Gidaris I, Taflanidis AA, Mavroeidis GP (2015): Kriging metamodeling in seismic risk assessment based on stochastic ground motion models. *Earthquake Engineering & Structural Dynamics*.**44** (14):2377-99.

[7] Padgett JE, DesRoches R (2008): Methodology for the development of analytical fragility curves for retrofitted bridges. *Earthquake Engineering & Structural Dynamics*.**37** (8):1157-74.

[8] Ryu H, Luco N, Uma S, Liel A (2011): Developing fragilities for mainshock-damaged structures through incremental dynamic analysis. *Ninth Pacific Conference on Earthquake Engineering, Auckland, New Zealand*.

[9] Luco N, Gerstenberger MC, Uma S, Ryu H, Liel AB, Raghunandan M (2011): A methodology for post-mainshock probabilistic assessment of building collapse risk. *Ninth Pacific Conference on Earthquake Engineering, Auckland, New Zealand*.

[10] Aslani H, Miranda E (2005): Probability-based seismic response analysis. *Engineering Structures*.**27** (8):1151-63.

[11] Jia G, Taflanidis AA (2013): Non-parametric stochastic subset optimization for optimal-reliability design problems. *Computers & structures*.**126**:86-99.

[12] Au S, Beck JL (1999): A new adaptive importance sampling scheme for reliability calculations. *Structural Safety*.**21** (2):135-58.

[13] Jia G, Taflanidis AA, Beck JL (2015): A new adaptive rejection sampling method using kernel density approximations and its application to Subset Simulation. *ASCE-ASME Journal of Risk and Uncertainty in Engineering Systems, Part A: Civil Engineering*.D4015001.

[14] Chang SE, Shinozuka M (2004): Measuring improvements in the disaster resilience of communities. *Earthquake Spectra*.**20** (3):739-55.

[15] Boore DM (2003): Simulation of ground motion using the stochastic method. *Pure and applied geophysics*.**160** (3-4):635-76.

[16] Atkinson GM, Silva W (2000): Stochastic modeling of California ground motions. *Bulletin of the Seismological Society of America*.**90** (2):255-74.

[17] Gidaris I, Taflanidis AA (2015): Performance assessment and optimization of fluid viscous dampers through life-cycle cost criteria and comparison to alternative design approaches. *Bulletin of Earthquake Engineering*.**13** (4):1003-28.

[18] Han R, Li Y, van de Lindt J (2016): Seismic Loss Estimation with Consideration of Aftershock Hazard and Post-Quake Decisions. *ASCE-ASME Journal of Risk and Uncertainty in Engineering Systems, Part A: Civil Engineering*.04016005.

[19] Song R, Li Y, Van de Lindt JW (2016): Loss estimation of steel buildings to earthquake mainshock–aftershock sequences. *Structural Safety*.**61**:1-11.

[20] Goda K (2012): Nonlinear response potential of mainshock–aftershock sequences from Japanese earthquakes. *Bulletin of the Seismological Society of America*.**102** (5):2139-56.

[21] Yeo GL, Cornell CA (2009): A probabilistic framework for quantification of aftershock ground-motion hazard in California: Methodology and parametric study. *Earthquake Engineering & Structural Dynamics*.**38** (1):45-60.

[22] Ramanathan K, Padgett JE, DesRoches R (2015): Temporal evolution of seismic fragility curves for concrete box-girder bridges in California. *Engineering Structures*.**97**:29-46.

[23] Kramer SL. Geotechnical earthquake engineering: Prentice Hall Upper Saddle River, NJ; 1996.

[24] Zhang J, Huo Y (2009): Evaluating effectiveness and optimum design of isolation devices for highway bridges using the fragility function method. *Engineering Structures*.**31** (8):1648-60.

[25] Decò A, Bocchini P, Frangopol DM (2013): A probabilistic approach for the prediction of seismic resilience of bridges. *Earthquake Engineering & Structural Dynamics*.**42** (10):1469-87.

[26] HAZUS-MH. Multi-Hazard Loss Estimation Methodology: Earthquake Model HAZUS-MH MR5 Technical Manual. Washington DC: Federal Emergency Management Agency; 2011.